Korean J. Chem. Eng., **30**(8), 1552-1558 (2013)
DOI: 10.1007/s11814-013-0087-7

Accuracy enhancement of thermal dispersion model in prediction of convective heat transfer for nanofluids considering the effects of particle migration

Mehdi Bahiraei*,,† and Seyed Mostafa Hosseinalipour****

*Department of Energy, Kermanshah University of Technology, Kermanshah, Iran
**CFD Lab & CAE Center, School of Mechanical Engineering, Iran University of Science & Technology, Narmak, Tehran, Iran
(*Received 22 February 2013 • accepted 16 May 2013*)

Abstract−A thermal dispersion model is utilized for simulation of convective heat transfer of water-TiO_2 nanofluid for laminar flow in circular tube. Concentration distribution at cross section of the tube was obtained considering the effects of particle migration, and this concentration distribution was applied in the numerical solution. Numerical solution was done at Reynolds numbers of 500 to 2000 and mean concentrations of 0.5 to 3%. Meanwhile, an experimental study was conducted to investigate the accuracy of the results obtained from the numerical solution. Non-uniformity of the concentration distribution increases with raising mean concentration and Reynolds number. Thereby, for mean concentration of 3%, at Reynolds numbers of 500 and 2000, the concentration from wall to center of the tube increases 2.6 and 30.9%, respectively. In the dispersion model, application of non-uniform concentration distribution improves the accuracy in prediction of the convective heat transfer coefficient in comparison with applying uniform concentration.

Key words: Water-TiO_2 Nanofluid, Non-uniform Concentration, Experimental, Heat Transfer, Particle Migration

INTRODUCTION

Owing to significant technological advancements, many devices have been developed which generate more heat at higher rate. The number of these devices has increased while they have been further improved. Therefore, heat transfer and cooling techniques must develop along with other sciences in order to properly dissipate the excess heat produced in such devices. Two general methods can be used for improving heat transfer: (1) Providing new designs for the cooling devices, such as microchannels and miniature cryodevices; (2) Improving heat transfer characteristics of the fluid itself. With regard to the latter method, thermal properties of the base fluid can be improved by adding solid particles to it. Suspension of nanoparticles in the conventional fluids is called nanofluid [1]. One of the most important observed characteristics is higher stability of the nanofluids in comparison with the suspensions containing micron-sized particles. Their other characteristic is their unexpectedly high thermal conductivity just by adding small amounts of nanoparticles [2-4].

Due to the excellent characteristics observed in nanofluids, several studies have been conducted on them in the numerical, analytical and experimental fields [5,6]. Considerable amount of effort has been made in order to numerically simulate flow and heat transfer of the nanofluids. Due to the very small size of the nanoparticles, some researchers have ignored thermal and hydrodynamic slips between the solid and liquid phases and have considered nanofluid as a homogeneous fluid [7-9]. It means that the effective properties are utilized in conservation equations. However, nanofluids are in fact two-phase media in which various phenomena occur. Buongiorno [10] introduced seven important mechanisms which affect heat transport in nanofluids. Brownian motion, nanoparticle migration and liquid layering at particle interface were addressed in other studies as factors affecting heat transport in nanofluids [11-13]. Therefore, considering the nanofluid as a homogeneous medium might neglect the effect of some phenomena in the simulation. Another approach for numerical simulation of the nanofluid is considering it as a two-phase medium. Some studies have shown that the single-phase methods provide less accurate results in comparison with the two-phase methods [14,15]. However, this approach also requires great volume and time of calculations. Some researchers have benefited from a third approach called thermal dispersion, which is based on the single-phase approach so it does not demand a great volume of calculations. On the other hand, the phenomena which can affect heat transport in nanofluids are also taken into account, considering the dispersion coefficient. In the conventional homogeneous approach, effective properties of nanofluid which are obtained in the stagnant state (u_{bulk}=0) are included into the conservation equations, whereas movement of the fluid can considerably affect the interaction between fluid and particles. In thermal dispersion method, it is tried to add a virtual term to the thermal conductivity of the nanofluid in order to take into account the effects associated with chaotic movements of the particles which were being neglected in the thermal conductivity. First time, Xuan and Roetzel [16] suggested a model for thermal dispersion based on porous media for nanofluid. They considered the thermal dispersion as a function of density, specific heat, velocity and volume fraction of nanofluid. After Xuan and Roetzel, some researchers have adopted this model in their simulations [17-19].

In the models which have so far been used for prediction of the dispersion coefficient in heat transfer simulation of nanofluids, distribution of the particles caused by particle migration has not been considered. In this study, we consider the effects of particle migra-

†To whom correspondence should be addressed.
E-mail: bahira@iust.ac.ir

tion, that can cause non-uniformity in the concentration distribution, in the thermal dispersion model.

DEFINITION OF GEOMETRY AND GOVERNING EQUATIONS

The geometry used in the present analysis was a circular tube. To reduce the volume of calculations, the problem has been solved axisymetrically. Due to the presence of more intensive velocity and temperature gradients near the wall, a finer meshing has been used there.

The conservation equations in the dispersion model are similar to those of the single-phase fluid, except that the effective thermophysical properties are used in these equations. The dispersion coefficient is also considered in the effective thermal conductivity which exists in the energy equation. The dimensional conservation equations for steady state conditions are listed below:

Continuity equation:

$$\nabla\cdot(\rho\mathbf{v})=0 \tag{1}$$

Momentum equation:

$$\nabla\cdot(\rho\mathbf{vv})=-\nabla P+\nabla\cdot(\mu\nabla\mathbf{v}) \tag{2}$$

Energy equation:

$$\nabla\cdot(\rho c_p\mathbf{v}T)=\nabla\cdot(k\nabla T) \tag{3}$$

where, ρ, c_p, k and μ represent density, specific heat, thermal conductivity and viscosity of the nanofluid, respectively.

1. Nanofluid Properties

Density and specific heat of the nanofluid are calculated based on concentration of the nanoparticles as below:

$$\rho=\varphi\rho_p+(1-\varphi)\rho_{bf} \tag{4}$$

$$c_p=\varphi c_{p,p}+(1-\varphi)c_{p,bf} \tag{5}$$

where p and bf subscripts refer to particle and base fluid, respectively, and φ denotes concentration. Thermal conductivity of the nanofluid is computed by the following equation:

$$k=k_{nf}+k_d \tag{6}$$

where k_{nf} is the thermal conductivity of the nanofluid without considering the effects of dispersion, which is obtained for stagnant state. k_d is the dispersion thermal conductivity which will be introduced later.

Hamilton-Crosser model [20] was used for the stagnant thermal conductivity.

$$k_{nf}=k_{bf}\frac{k_p+(n-1)k_{bf}-(n-1)\varphi(k_{bf}-k_p)}{k_p+(n-1)k_{bf}+\varphi(k_{bf}-k_p)} \tag{7}$$

where n is equal to 3 for spherical particles.

For viscosity, our measured data were used, while Eq. (8) was obtained in terms of temperature and concentration by applying curve fitting on these data. An experimental setup equipped with a constant temperature bath was used where a glass viscometer was placed inside the bath. Detailed specifications of the experimental setup have been explained completely in our previous work [21]. To ensure the accurate operation of the experimental setup, prior to measurement of the viscosity of water-TiO_2 nanofluid, the viscosity of pure water was measured and compared with the reliable values [22] which reported an average error content of approximately 1%. The correlation extracted from the regression for water-TiO_2 nanofluid is given as below:

$$\mu=0.009093894T^{-0.721707}(\varphi+1)^{0.258153} \tag{8}$$

where T is temperature of the nanofluid in Celsius.

2. Boundary Conditions

The developed velocity profile was applied at the tube inlet. Zero relative pressure at the tube outlet was considered along with no slip condition at the tube wall. Uniform temperature was employed at the inlet, while constant heat flux was applied on the wall.

NUMERICAL METHOD AND VALIDATION

Control volume technique was used to discretize the equations with second-order upwind scheme. Meanwhile, *SIMPLE* method was employed for velocity-pressure coupling. Different meshes with various numbers of cells were used to ensure the grid independency. A mesh with 25 nodes in the radial direction and 2500 nodes in the axial direction was selected as the appropriate meshing. To insure the numerical method and appropriateness of the meshes, the results from the numerical solution for pure water were compared with the reliable results [23] at Re=1500. From Fig. 1, the results are consistent and thus the numerical solution is valid.

THERMAL DISPERSION MODEL

Since the particles in nanofluids are extremely fine, chaotic motion of particles can affect the heat transport significantly. Especially when the nanofluid is flowing, the interaction between particles and fluid can be different from stagnant state of the nanofluid. Thermal dispersion occurs in flow field of the nanofluid, which alters the distribution of temperature and affects the heat transfer content. Random movements of particles cause small perturbations in both fields of velocity and temperature, i.e., $\mathbf{v}'$ and T', respectively.

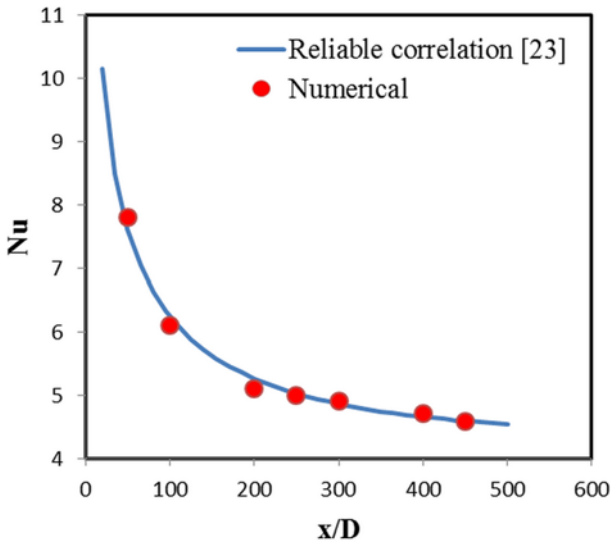

Fig. 1. Validation of numerical method in comparison with a reliable correlation [23] for water at Re=1500.

Intrinsic phase averages are given by Xuan and Roetzel [16]:

$$\mathbf{v}=\overline{\mathbf{v}}+\mathbf{v}' \tag{9}$$

$$T=\overline{T}+T' \tag{10}$$

Where:

$$\overline{\mathbf{v}}=\frac{1}{V_f}\int_{V_f}\mathbf{v}dV \tag{11}$$

$$\overline{T}=\frac{1}{V_f}\int_{V_f}TdV \tag{12}$$

According to the procedure described by Kaviany [24] and also neglecting the small boundary surface between the fluid and the particles, one can put forward the equation below for the energy equation by substituting Eqs. (9) and (10) in Eq. (3):

$$\nabla\cdot(\rho c_p\overline{\mathbf{v}}\overline{T})=\nabla\cdot k_{nf}\nabla\overline{T}-\nabla\cdot(\rho c_p\overline{\mathbf{v}'T'}) \tag{13}$$

The second term on the right side of Eq. (13) represents the perturbation effect of velocity and temperature in energy equation. This term demonstrates the effect of thermal dispersion resulting from chaotic and random motion of the nanoparticles within the flow. Similar to the behavior of turbulent flow, heat flux induced by the thermal dispersion in nanofluid flow can also be expressed as:

$$\rho c_p\overline{\mathbf{v}'T'}=-k_d\nabla\overline{T} \tag{14}$$

Eq. (13) can be rewritten as below:

$$\nabla\cdot(\rho c_p\overline{\mathbf{v}}\overline{T})=\nabla\cdot(k_{nf}+k_d)\nabla\overline{T} \tag{15}$$

In fact, k_d is a virtual term rather than a fluid property. It is added to the thermal conductivity of the nanofluid to take into account the heat transport caused by the thermal dispersion. In the models suggested so far for k_d, concentration has been considered to be uniform with the effect of particle migration being ignored in it.

The current research provides the correlation below for the dispersion thermal conductivity in radial direction:

$$k_d=c\rho c_p\left(\frac{\partial v_x}{\partial r}\right)\varphi(r)Rd_p \tag{16}$$

where c is an empirical coefficient obtained from the comparison with experimental results. R and d_p represent radius of the pipe and size of particles, respectively. The distribution of concentration (φ(r)) has been applied in addition to inclusion of velocity gradient in this model. Thus, concentration distribution must be evaluated for being used in the model.

DISTRIBUTION OF PARTICLE CONCENTRATION

The distribution of concentration is affected by three mechanisms in non-uniform shear flows: viscosity gradient-induced migration, shear-induced migration and self-diffusion caused by Brownian motion.

For a steady-state and fully developed nanofluid flow through a horizontal pipe, establishing a mass balance for the particle phase will yield [13]:

$$J+r\frac{dJ}{dr}=0 \tag{17}$$

where r is the radial coordinate and J is the total flux of particles in r direction. Eq. (17) presumes particle phase as continuous. As discussed above, the total flux of particle migration contains three terms:

$$J=J_\mu+J_c+J_b \tag{18}$$

where J_μ, J_c and J_b denote the particle fluxes occurred as a result of viscosity gradient, non-uniform shear rate and Brownian motion, respectively. Correlating with experimental data, Phillips et al. [25] proposed the following equations:

$$J_\mu=-K_\mu\dot{\gamma}\varphi^2\left(\frac{d_p^2}{\mu}\right)\frac{d\mu}{d\varphi}\nabla\varphi \tag{19}$$

$$J_c=-K_c d_p^2(\varphi^2\nabla\dot{\gamma}+\varphi\dot{\gamma}\nabla\varphi) \tag{20}$$

$$J_b=-D_B\nabla\varphi \tag{21}$$

where K_μ and K_c are constants, $\dot{\gamma}$ represents the shear rate and D_B gives the Brownian diffusion coefficient calculated by:

$$D_B=\frac{k_BT}{3\pi\mu d_p} \tag{22}$$

where k_B is Boltzmann's constant. Integrating Eq. (17) using symmetrical boundary condition at r=0, will produce the following equation:

$$J=J_\mu+J_b+J_c=0 \tag{23}$$

By substituting Eqs. (19)-(21) into Eq. (23) and also adopting Newtonian model for the nanofluid, one would find:

$$\frac{1}{\mu}\frac{d\mu}{d\bar{r}}+\left(\frac{K_c}{K_\mu}\right)\frac{\mu}{\bar{r}}\frac{d\left(\frac{\bar{r}}{\mu}\right)}{d\bar{r}}+\left(\frac{K_c}{K_\mu}\right)\frac{1}{\varphi}\frac{d\varphi}{d\bar{r}}+\frac{2k_BT}{3\pi K_\mu d_p^3(dp/dz)R\varphi^2\bar{r}}\frac{d\varphi}{d\bar{r}}=0 \tag{24}$$

where: $\bar{r}=\frac{r}{R}$

A boundary condition is required to solve Eq. (24) which is generated by Eq. (25) as follows:

$$\varphi_m=\frac{\int\varphi(r)dA}{\int dA} \tag{25}$$

where φ_m is the mean concentration.

Solution of Eq. (24) introduces the concentration distribution of

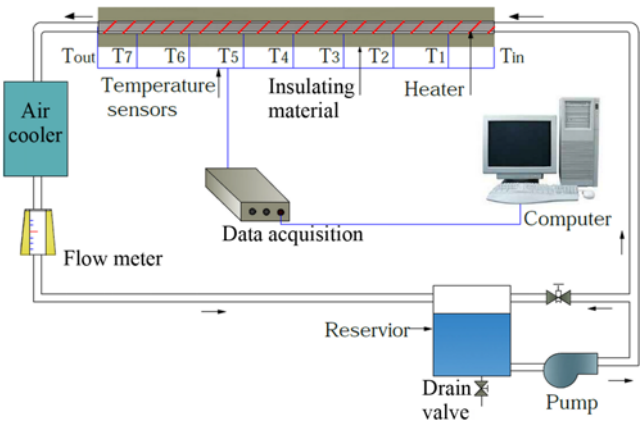

Fig. 2. Schematic view of experimental setup.

particles in a fully developed region of the pipe. This study uses the obtained concentration distribution from Eq. (24) in Eq. (16) for dispersion thermal conductivity.

EXPERIMENTAL SETUP

To find the empirical coefficient in the dispersion model and to investigate the accuracy of the results obtained from the numerical simulation, we implemented an experimental study. For this purpose, the setup of Fig. 2 was utilized, in which uniform heat flux was used for heating the tube wall. Seven *pt-100* temperature sensors were employed to measure surface temperature. These sensors were installed with the same distances on the tube. Data from these sensors were monitored and recorded by a data acquisition system. For the experiments, water-TiO_2 nanofluid was prepared through a two-step method at concentrations of 0.5, 1.5 and 3 vol%. In this regard and after the nanoparticles were mixed in the base fluid by a magnetic stirrer, ultrasonic waves were applied in an ultrasonic mixer to disperse the particles in the liquid phase and also to break up agglomerated nanoparticles. The produced nanofluid showed a very good stability, such that no sign of settlement was observed even after several months under static condition.

Nusselt number obtained from the experimental results was compared with that of a reliable correlation [23] at Re=1000 for pure water in order to ensure proper performance of the setup (Fig. 3). It is evident that there is a good agreement between the results. Therefore, the results of this setup are rated valid.

After validation of the experimental setup, each test was conducted twice for the nanofluid, and since the difference between the results was very low, their average values were considered. In this study, the uncertainty in measurement of the convective heat transfer coefficient may result from the measuring errors of parameters such as temperature, flow rate and heat flux (Eq. (26)).

$$\frac{\delta h}{h}=\sqrt{\left(\frac{\delta T}{T}\right)^2+\left(\frac{\delta q''}{q''}\right)^2+\left(\frac{\delta \dot{m}}{\dot{m}}\right)^2} \tag{26}$$

where, q'' denotes wall heat flux and $\dot{m}$ represents flow rate.

The errors of temperature reading from calibrated *pt-100* sensor and the measured flow rate were less than 0.1% and 1%, respectively. Moreover, the error for the heat flux was less than 2%. Hence, the uncertainty of the measured convective heat transfer coefficient is assessed less than 3%.

RESULTS AND DISCUSSION

Distribution of concentration at the cross section of the tube for water-TiO_2 nanofluid from solution of Eq. (24) has been depicted in Fig. 4 for different mean concentrations at Re=1500. Increasing the mean concentration intensifies non-uniformity of the concentration distribution. The distribution of concentration from solving Eq. (24) for different Reynolds numbers at φ_m=3% has been illus-

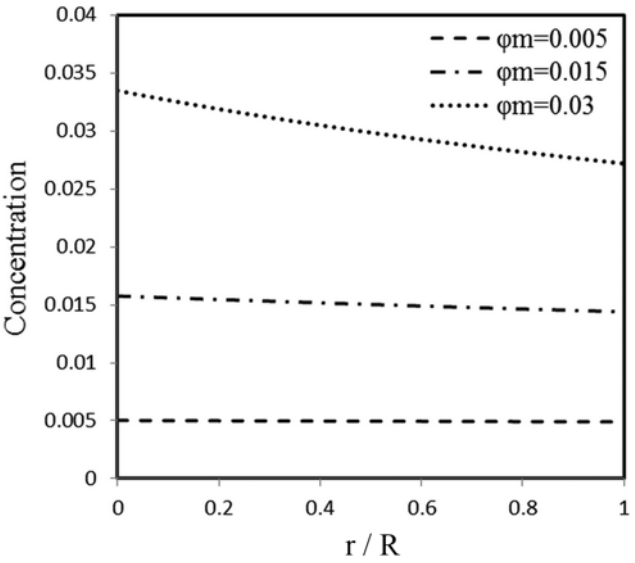

Fig. 4. Distribution of concentration at the cross section of the tube for different mean concentrations at Re=1500.

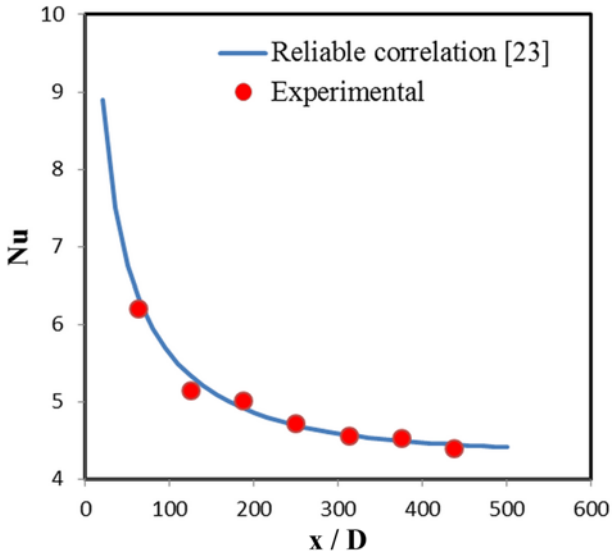

Fig. 3. Validation of experimental setup in comparison with a reliable correlation [23] for pure water at Re=1000.

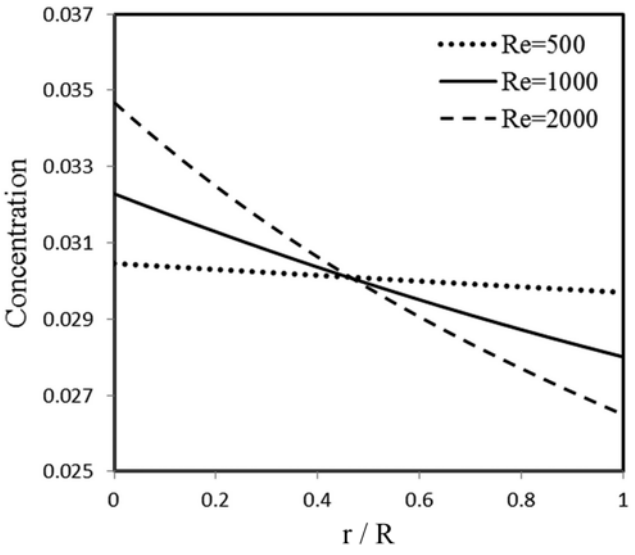

Fig. 5. Distribution of concentration at the cross section of the tube for different Reynolds numbers at φ_m=3%.

trated in Fig. 5. A more non-uniform distribution of concentration is obtained at greater Reynolds numbers. Thereby, at Reynolds numbers of 500 and 2000, the concentration from wall to center of the tube increases about 2.6 and 30.9%, respectively. Maximum content of concentration occurs in the center of the tube for all states. The values applied in the study conducted by Wen and Ding [26] were used for the existing constants in Eq. (24).

Fig. 6 shows the convective heat transfer coefficient of the nanofluid at Re=1000 and φ_m=1.5% for conditions of applying uniform and non-uniform concentrations in the simulation as compared with the experimental results. The results obtained from applying the non-uniform concentration are in a good agreement with the experimental results. However, application of the uniform concentration

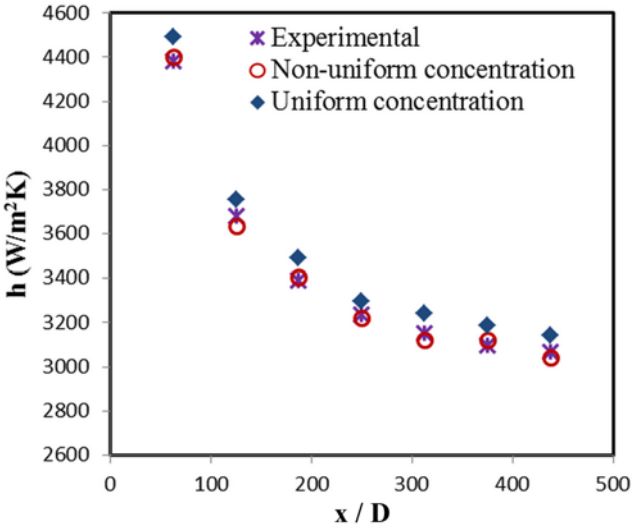

Fig. 6. Convective heat transfer coefficient of nanofluid for conditions of applying uniform and non-uniform concentrations at Re=1000 and φ=1.5% in comparison with the experimental results.

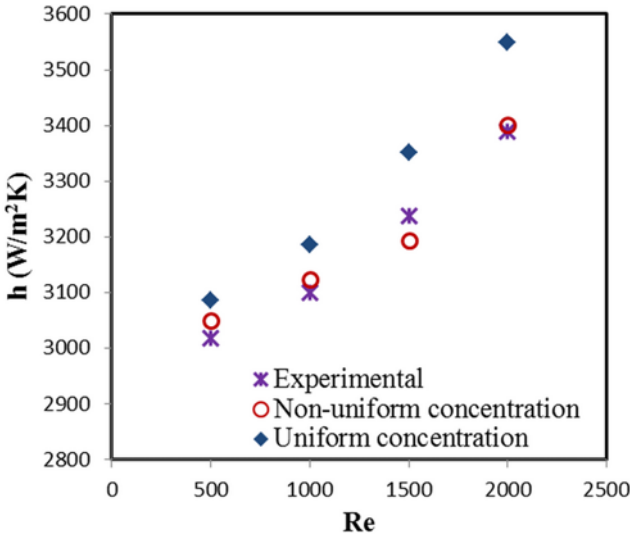

Fig. 7. Convective heat transfer coefficient of nanofluid from numerical simulation at x/D=375 and φ=1.5% versus Reynolds number in comparison with the experimental results.

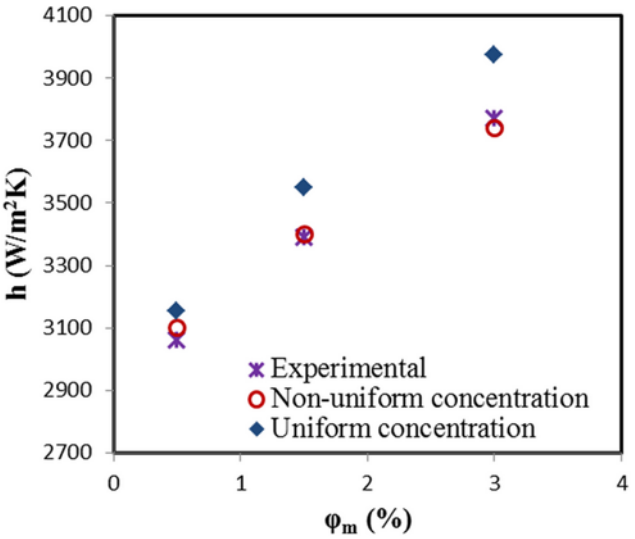

Fig. 8. Convective heat transfer coefficient of nanofluid from numerical simulation at x/D=375 and Re=2000 versus mean concentration in comparison with the experimental results.

in solution overestimates the experimental results. This phenomenon can be attributed to the fact that at a similar mean concentration, the value of concentration at the wall vicinity for uniform concentration is greater than that of non-uniform concentration. On the other hand, thermal conductivity of the nanofluid depends on the concentration content.

Fig. 7 depicts the convective heat transfer coefficient of the nanofluid from numerical simulation at x/D=375 and φ=1.5% versus Reynolds number in comparison with the experimental results. One can easily notice that the accuracy of the results applying the uniform concentration was reduced by increasing the Reynolds number. This is because increasing the Reynolds number will intensify non-uniformity of the concentration as demonstrated in Fig. 5, whereas application of a non-uniform concentration in the dispersion model has provided acceptable results at all Reynolds numbers.

Fig. 8 illustrates the convective heat transfer coefficient of the nanofluid versus mean concentration at x/D=375 and Re=2000. In comparison with the experimental results, the accuracy of the dispersion model which has used a uniform concentration is reduced at higher mean concentrations. This is because raising the mean concentration will intensify the non-uniformity of the concentration at the cross section of the tube (according to Fig. 4). However, the results of the dispersion model which has considered a non-uniform distribution for the concentration are much closer to the experimental results, even at high mean concentrations.

Fig. 9 depicts the temperature and velocity profiles at the cross section of the pipe for cases of applying uniform and non-uniform concentration distributions at φ=3% and Re=2000. As illustrated in Fig. 9(a), for non-uniform concentration, the temperature gradients at the wall vicinity and central regions are, respectively, more intense and smoother as compared with the case of uniform concentration. The reason is that in the case of non-uniform concentration, the thermal conductivity at the wall vicinity and tube central regions is, respectively, lower and higher in comparison with the case of uniform concentration. Furthermore, the nanofluid temper-

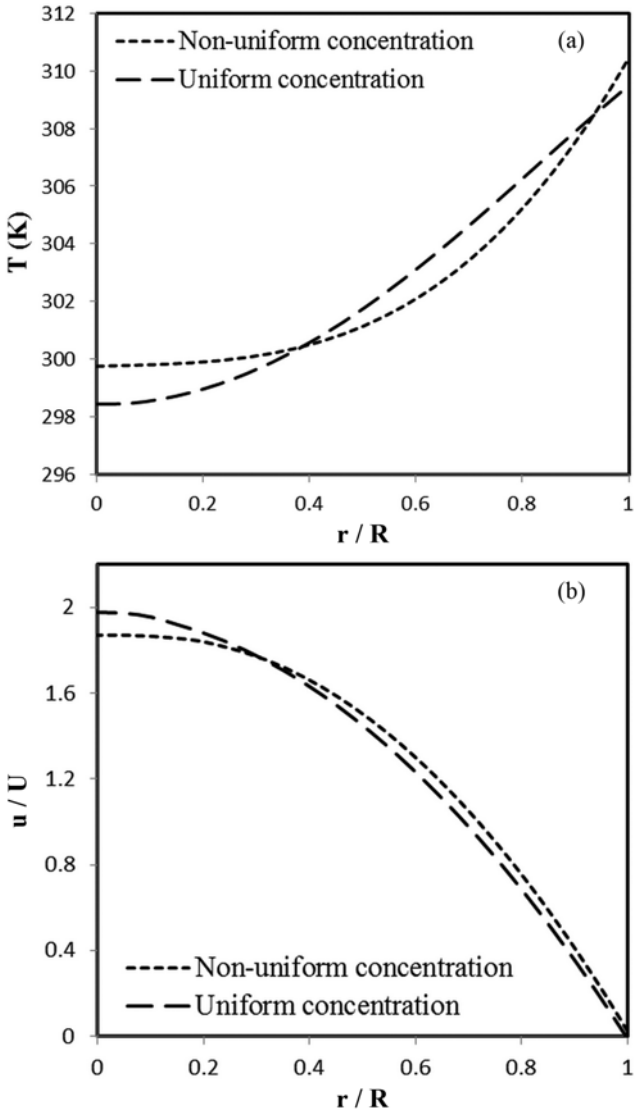

Fig. 9. Profiles of (a) temperature and (b) velocity; at φ=3% and Re=2000 for cases of applying uniform and non-uniform concentrations.

ature near the wall (i.e., at r/R=1) is lower for uniform concentration. It means that the surface temperature of the pipe is lower in this case, and consequently according to Eq. (27), higher convective heat transfer coefficient is obtained in the case of uniform concentration which has been shown in Figs. 6-8.

$$h = \frac{k\partial T/\partial r|_{r=R}}{T_s - T_m} \tag{27}$$

where, T_s and T_m represent the surface temperature and the bulk temperature of the nanofluid, respectively.

In addition, the temperature of the nanofluid at central regions of the pipe is higher in the case of non-uniform concentration in comparison with the uniform one. A reason for such an observation can be the lower specific heat of the nanofluid (c_p) at central regions for the case of non-uniform concentration, since in this case, the concentration is higher at the central regions and on the other hand, the specific heat of TiO_2 is lower than that of the water.

As shown in Fig. 9(b), for non-uniform concentration, the dimensionless velocity profile is flatter than that of the uniform concentration. The reason is that in the case of non-uniform concentration, as was shown in Figs. 4 and 5, the concentration is higher at the central regions of the pipe; thus, the viscosity and consequently resistance to the fluid motion is higher there. Hence, the fluid velocity decreases at the central regions while increasing near the wall.

From Figs. 6 to 8, it can be inferred that application of the particle migration effects in the simulation, which has been considered in this study through using a non-uniform concentration, improves the accuracy of the dispersion model.

CONCLUSION

The distribution of concentration has been used in the thermal dispersion model to simulate heat transfer of water-TiO_2 nanofluid to take into account the factors affecting the particle migration. A more non-uniform distribution of concentration was obtained at higher Reynolds numbers and greater mean concentrations. Therefore, application of a uniform concentration in the dispersion model will cause greater errors at higher Reynolds numbers and mean concentrations. Comparing the results of numerical simulation with those of the experimental work revealed that the dispersion model, which adopts a non-uniform concentration, is more promising than that of considering a uniform concentration.

NOMENCLATURE

A : area [m^2]
c : empirical coefficient
c_p : specific heat [J/kgK]
D_B : Brownian diffusion coefficient [m^2/s]
d : diameter [m]
h : convective heat transfer coefficient [W/m^2K]
J : total flux of particles [m/s]
K_μ : constant
K_c : constant
K_B : Boltzmann's constant [J/K]
k : thermal conductivity [W/mK]
$\dot{m}$: flow rate [kg/s]
P : pressure [Pa]
q″ : wall heat flux [W/m^2]
R : radius of tube [m]
Re : Reynolds number
r : radial coordinate
T : temperature [K]
T′ : temperature perturbation [K]
t : time [s]
V : volume [m^3]
v : velocity [m/s]
v′ : velocity perturbation [m/s]
z : axial direction

Greek Letters

$\dot{\gamma}$: shear rate [1/s]
μ : dynamic viscosity [kg/ms]
ρ : density [kg/m^3]

φ : volume fraction

Subscripts

bf : base fluid
d : dispersion
m : mean
nf : nanofluid
p : particle
s : surface

REFERENCES

1. S. Lee, S. U. S. Choi, S. Li and J. A. Eastman, *J. Heat Transf.*, **121**, 280 (1999).
2. S. K. Das, N. Putra, P. Thiesen and W. Roetzel, *J. Heat Transf.*, **125**, 567 (2003).
3. S. M. S. Murshed, K. C. Leong and C. Yang, *Int. J. Therm. Sci.*, **44**, 367 (2005).
4. J. A. Eastman, S. U. S. Choi, S. Li, W. Yu and L. J. Thompson, *Appl. Phys. Lett.*, **78**, 718 (2001).
5. B. H. Chun, H. U. Kang and S. H. Kim, *Korean J. Chem. Eng.*, **25**, 966 (2008).
6. S. Kim, H. Yoo and C. Kim, *Korean J. Chem. Eng.*, **29**, 1321 (2012).
7. V. Bianco, F. Chiacchio, O. Manca and S. Nardini, *Appl. Therm. Eng.*, **29**, 3632 (2009).
8. J. Koo and C. Kleinstreuer, *Int. J. Heat Mass Transf.*, **48**, 2652 (2005).
9. P. R. Mashaei, S. M. Hosseinalipour and M. Bahiraei, *J. Appl. Math.*, **2012**, 259284 (2012).
10. J. Buongiorno, *J. Heat Transf.*, **128**, 240 (2006).
11. J. Koo and C. Kleinstreuer, *Int. Commun. Heat Mass Transf.*, **32**, 1111 (2005).
12. Q. Z. Xue, *Phys. Lett. A*, **307**, 313 (2003).
13. Y. Ding and D. Wen, *Powder Tech.*, **149**, 84 (2005).
14. R. Lotfi, Y. Saboohi and A. M. Rashidi, *Int. Commun. Heat Mass Transf.*, **37**, 74 (2010).
15. M. Haghshenas Fard, M. Nasr Esfahany and M. R. Talaie, *Int. Commun. Heat Mass Transf.*, **37**, 91 (2010).
16. Y. Xuan and W. Roetzel, *Int. J. Heat Mass Transf.*, **43**, 3701 (2000).
17. S. Kumar, S. Kumar Prasad and J. Banerjee, *Appl. Math. Model.*, **34**, 573 (2010).
18. S. Z. Heris, M. N. Esfahany and G. Etemad, *Num. Heat Transf.*, **52**, 1043 (2007).
19. A. Mokmeli and M. Saffar-Avval, *Int. J. Therm. Sci.*, **49**, 471 (2010).
20. R. L. Hamilton and O. K. Crosser, *Ind. Eng. Chem. Fundam.*, **1**, 187 (1962).
21. M. Bahiraei, S. M. Hosseinalipour, K. Zabihi and E. Taheran, *Adv. Mech. Eng.*, **2012**, 742680 (2012).
22. R. W. Fox, A. T. McDonald and P. J. Pritchard, *Introduction to fluid mechanics*, Wiley, New York (2004).
23. A. Bejan and A. D. Kraus, *Heat transfer handbook*, Wiley, New York (2003).
24. M. Kaviany, *Principles of heat transfer in porous media*, Springer, New York (1995).
25. R. J. Phillips, R. C. Armstrong, R. A. Brown, A. L. Graham and J. R. Abbott, *Phys. Fluids, A Fluid Dyn.*, **4**, 30 (1992).
26. D. Wen and Y. Ding, *Microfluid. Nanofluid.*, **1**, 183 (2005).